

Phase transitions of correlated systems from graph neural networks with quantum embedding techniques

Rishi Rao and Li Zhu*

Department of Physics, Rutgers University, Newark, New Jersey 07102, USA

(Dated: April 16, 2024)

Correlated systems represent a class of materials that are difficult to describe through traditional electronic structure methods. The computational cost of simulating the structural dynamics of such systems, with correlation effects considered, is substantial. Here, we investigate the structural dynamics of f - and d -electron correlated systems by integrating quantum embedding techniques with interatomic potentials derived from graph neural networks. For Cerium, a prototypical correlated f -electron system, we use Density Functional Theory with the Gutzwiller approximation to generate training data due to efficiency with which correlations effects are included for large multi-orbital systems. For Nickel Oxide, a prototypical correlated d -electron system, advancements in computational capabilities now permit the use of full Dynamical Mean Field Theory to obtain energies and forces. We train neural networks on this data to create a model of the potential energy surface, enabling rapid and effective exploration of structural dynamics. Utilizing these potentials, we delineate transition pathways between the α , α' , and α'' phases of Cerium and predict the melting curve of Nickel Oxide. Our results demonstrate the potential of machine learning potentials to accelerate the study of strongly correlated systems, offering a scalable approach to explore and understand the complex physics governing these materials.

Strongly correlated systems, characterized by significant electron-electron interactions, present a frontier in materials science and condensed matter physics. These interactions lead to phenomena like Mott transitions [1, 2], heavy fermion behavior [3–5], spin-charge separation [6, 7] and other correlation induced effects that can be technologically useful and physically interesting [8–12]. Conventional computational methods for dealing with interactions, such as Dynamical Mean Field Theory (DMFT) [13, 14], Density Matrix Renormalization Groups (DMRG) [15, 16], Gutzwiller wavefunction techniques [17, 18], and Hubbard U corrections to Density Functional Theory (DFT) [19, 20], have advanced our understanding of the electronic structures of such materials. However, simulating the structural dynamics and thermodynamics of strongly correlated materials remains a significant challenge due to the computational cost associated with the large Hilbert spaces that arise from many-body electron-electron interactions [21, 22]. As the number of interactions increase, the size of the Hilbert space rapidly increases as well. This expansion makes the calculation of dynamics particularly tedious for correlated systems, as dynamics generally require extensive sampling over many structural configurations.

This computational bottleneck becomes particularly prohibitive when exploring structural phase transitions and conducting molecular dynamics (MD) simulations. Although methods like DMFT and DMRG can offer nearly quantitative accuracy, their scalability issues and the technical difficulties in applying these approaches to multi-dimensional and large multi-orbital systems limit their practicality for direct studies of structural dynamics. For example, the exact method for solving the DMFT

impurity problem, the continuous time quantum monte carlo (CTQMC) algorithm [23–25], samples Feynman diagrams to arbitrary order in imaginary time. This suffers from an exploding number of Monte Carlo steps required to accurately gauge the self energy as temperature is lowered or when considering a greater number of orbitals. Similarly, DMRG becomes technically difficult to implement in more than two dimensions [26]. Techniques like the Hubbard U correction, while useful, often lack the quantitative accuracy needed for predicting complex behaviors under varying conditions such as high pressure [27], and are less quantitatively accurate than DMFT [28, 29]. The Gutzwiller approximation technique, equivalent to a mean field approximation of slave boson techniques in the limit of infinite spatial dimensions [30–32], has been successfully applied to numerous correlated systems [33–39] and provides a relatively cheap way method for tackling large multi-orbital systems. However, even this method is significantly more computationally expensive than traditional DFT as it provides iterative corrections to a tight-binding Hamiltonian generated from DFT.

These computational challenges are significant in studying materials like Cerium (Ce) and Nickel Oxide (NiO), which exhibit interesting properties under extreme conditions. Cerium, known for its complex structural phase transitions under intermediate pressure, exemplifies the challenges associated with accurately determining the lowest energy phase under varying pressure and temperature conditions. These phases are critical for understanding its properties and potential applications, yet first-principles study is hampered by the prohibitive computational cost of simulating strong correlation effects. Similarly, determining the melting point of compounds like NiO, an important component of the lower mantle of Earth [40–42], under high pressures is crucial

* li.zhu@rutgers.edu

for understanding the dynamics and properties near the Earth’s core. Traditional DFT methods fall short of accurately predicting the electronic structure of NiO and Ce due to strong correlation effects, underscoring the need for more advanced simulation techniques.

In response to these challenges, this study introduces a novel approach that leverages machine learning (ML) to develop interatomic potentials from beyond-DFT methods, aiming to transform the study of strongly correlated systems. By combining quantum embedding techniques with the robust interpolation capabilities of graph neural networks, we propose a method to significantly reduce the time associated with simulating the structural properties of these complex materials. Specifically, we focus on the multi-orbital Gutzwiller approximation for f -electron materials and DFT+DMFT for d -electron materials as computationally tractable methods to generate the initial training data for our ML models. This approach enables us to capture the essential physics of correlated systems with distributed computational cost, offering a promising pathway to accurately simulate phase transitions in Ce and the melting behavior of NiO under extreme conditions. Through the innovative use of machine learning interatomic potentials (MLIPs), we offer a scalable approach to explore and understand the complex physics governing strongly correlated materials, contributing to the accelerated development of novel materials with desirable properties.

Local Density Approximation (LDA) calculations were carried out using the augmented plane wave plus local orbital method, as implemented in the WIEN2K 23.2 package [43]. For Ce, a muffin tin radius of 2.5 Bohr was utilized, while for Ni and O, the radii were set to 1.8 Bohr and 1.5 Bohr, respectively. The smaller muffin tin radii for the NiO system accommodated high-pressure calculations. RKMax was set to 8.5 for the Ce system and 7.5 for the NiO system. LDA calculations were converged to a charge density within 10^{-3} and energy within 10^{-3} Rydberg. DMFT calculations for both systems were carried out using the eDMFT package [44, 45], with the impurity problem solved through a Continuous Time Quantum Monte Carlo solver [46]. Forces were obtained as a derivative of the Luttinger-Ward functional with respect to atomic positions [47].

For the Cerium system, charge self-consistent Gutzwiller calculations were carried out using the CyGutz package as implemented in [32, 48] until energy change was less than 5×10^{-4} Rydberg. The Hubbard U parameter chosen was 6.0 eV with a Hund coupling of 0.7 eV since previous studies indicate these values provide good agreement with experimental lattice parameters [49, 50]. Approximately 1500 sample points were generated near the relevant transition pathway. Structures were interpolated between the 2 stable phases and random perturbations of cell vectors and atomic positions were performed to get a wide range of possible structures. The resulting energies were used to train a graph neural network using the M3GNET package [51]. The MLIP was

trained until the mean average error of the energies was less than 50 meV/atom. Since force data is not yet easily obtainable within the Gutzwiller approximation, the finite difference method was used to calculate the forces and unit cell stresses.

The solid state NEB method was then used to discover transition pathways between stable structures as described in Ref. [52]. The pathways found were checked using charge self-consistent DMFT. We checked the pathways at temperatures of 116 K and 400 K for the impurity solver with 1.28×10^9 Monte Carlo steps split across 16 processors. Results converged on average at 10 charge-self consistency steps defined as the point when variation of the energy dropped below 10^{-3} eV. The same values of Coulomb repulsion and Hund’s coupling used for the Gutzwiller solver were used for the DMFT calculations. We employed nominal double counting as described in Refs. [44, 53, 54] to correct for the double contribution to the energy from both the LDA and DMFT solvers with a nominal value of 1.0 for Ce. Nominal double counting has been shown to perform better than the fully localized limit method used in many other studies [54].

For Nickel Oxide, full DMFT calculations were carried out to compute energies and forces. A Coulomb repulsion value of 8.0 eV and Hund coupling of 0.9 eV were chosen as they have been found to provide a good description of the electronic structure of NiO within DMFT at high pressures [55]. A double counting value of 8.0 was chosen and calculations were carried out at a temperature of 611 K, which is above the Neel temperature of NiO. Approximately 8×10^8 Monte Carlo steps were sampled, split across 8 processors. Data points were generated by randomly perturbing atomic positions and cell parameters, such as angles and lengths, of the face centered cubic structure. Molecular dynamics simulations were carried out using the atomic simulation environment package (ASE) [56] in the NVE ensemble to investigate the evolution of the melting curve under pressure using the Z-method [57, 58]. Experimental volume-pressure relations were compared to DFT calculations from the VASP package [59–61] using a plane-wave basis set with Planar augmented wave pseudopotentials [62–64] and an exchange-correlation functional based on a revised Perdew-Burke-Ernzerhof for solids (PBEsol) version of the generalized gradient approximation [65].

As a prototypical correlated f -electron material, elemental Ce has been extensively studied for decades [67–69], with computational focus directed at the isostructural $\gamma \rightarrow \alpha$ transition, which has been described as a collapse due the large decrease in volume ($\approx 17\%$) as pressure increases past 0.8 GPa [70]. Efforts have also been made to explore the intermediate pressure phases of Ce within the 5-12 GPa range, where it typically undergoes a structural phase transition from a face-centered cubic phase ($Fm\bar{3}m$, α -Ce) to either a monoclinic ($C2/m$, α'' -Ce) or orthorhombic ($Cmcm$, α' -Ce) phase, depending on sample preparation conditions [71–73]. However, the stability and synthesis conditions for these intermediate-

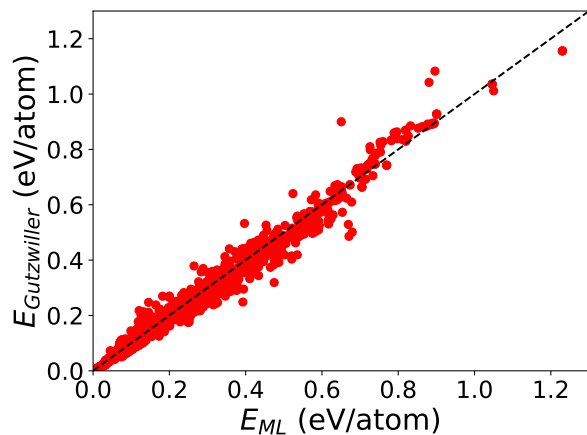


FIG. 1. Internal energies predicted by the MLIP versus energies calculated by solving tight binding model with Gutzwiller approximation. Black dashed line represents perfect agreement.

pressure pathways remain ambiguous. Some studies advocate for the monoclinic phase as most stable [74, 75] while others argue that the orthorhombic phase [76, 77] is most stable at these conditions. Recent investigations suggest that the orthorhombic phase is favored at higher temperatures, whereas cold-working tends to stabilize the monoclinic phase [72]. There is a notable scarcity of computational studies investigating the transition pathways for these phase transformations. Traditional DFT struggles to account for the correlation effects present in Ce, and beyond DFT methods are required for accurate descriptions of the potential energy surface. In addressing the computational complexity associated with exploring these transition pathways, our study employs a MLIP, trained with data from LDA+Gutzwiller calculations, to investigate the transition pathways from the α phase to these intermediate pressure phases.

Predicted energies from our interatomic potential are in agreement with those obtained from the Gutzwiller solver, as demonstrated in our results (Fig. 1). While higher energy phases show more errors, the accuracy for low energy structures (critical for transition pathways) is quite high, which lends confidence to our computational predictions, as transition pathways are typically comprised of structures from the low energy regime. Using the solid-state NEB method, we explored transitions under 7.5 GPa of pressure and checked the results using a full DMFT treatment calculated at 116 K and 400 K. At the lower temperature of 116 K (Fig. 2a), the α phase is predicted to transition to the monoclinic α'' phase, which has the lowest Gibbs free energy. The transition to the orthorhombic α' -Ce phase, while still exothermic, involves a higher reaction barrier and higher Gibbs free energy at 116 K, suggesting a less favored phase transition under these conditions. These findings agree with the experimental observations and support the hypothesis that cold-worked samples prefer the monoclinic phase,

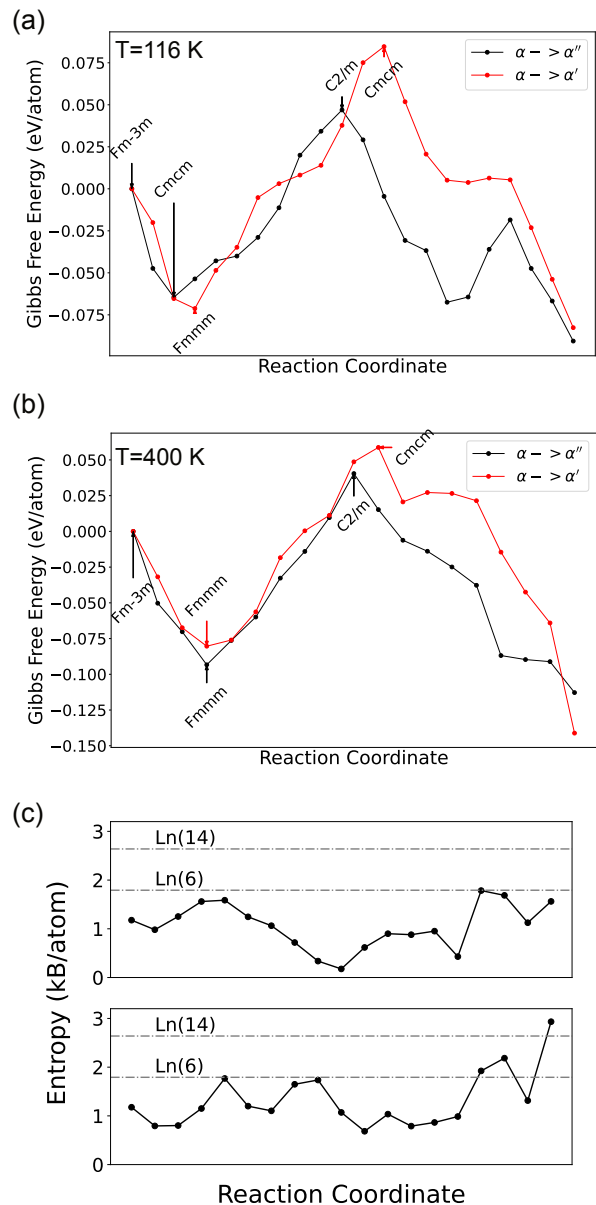


FIG. 2. Gibbs Free Energy per atom for the $\alpha \rightarrow \alpha''$ (black) and $\alpha \rightarrow \alpha'$ (red) transition pathways at a pressure of 7.5 GPa, calculated using single-site DMFT at a temperature of 116 K (a) and 400 K (b). (c) Entropy per atom for the $\alpha \rightarrow \alpha''$ (top) and $\alpha \rightarrow \alpha'$ (bottom) transition pathways at 7.5 GPa of pressure calculated using single-site DMFT at a temperature of 400 K.

as it has the lowest Gibbs free energy at 116 K.

As the temperature increases to 400 K, the energy landscape alters noticeably (Fig. 2b). The reaction barriers to both the α'' and α' phases decrease, and the energy profiles of the two phases are very close, especially between the α phase and the transition states. This closeness suggests a competitive mechanism at play. However, the orthorhombic α' -Ce phase becomes the lowest energy state, indicating an increased likelihood of obtaining α' -

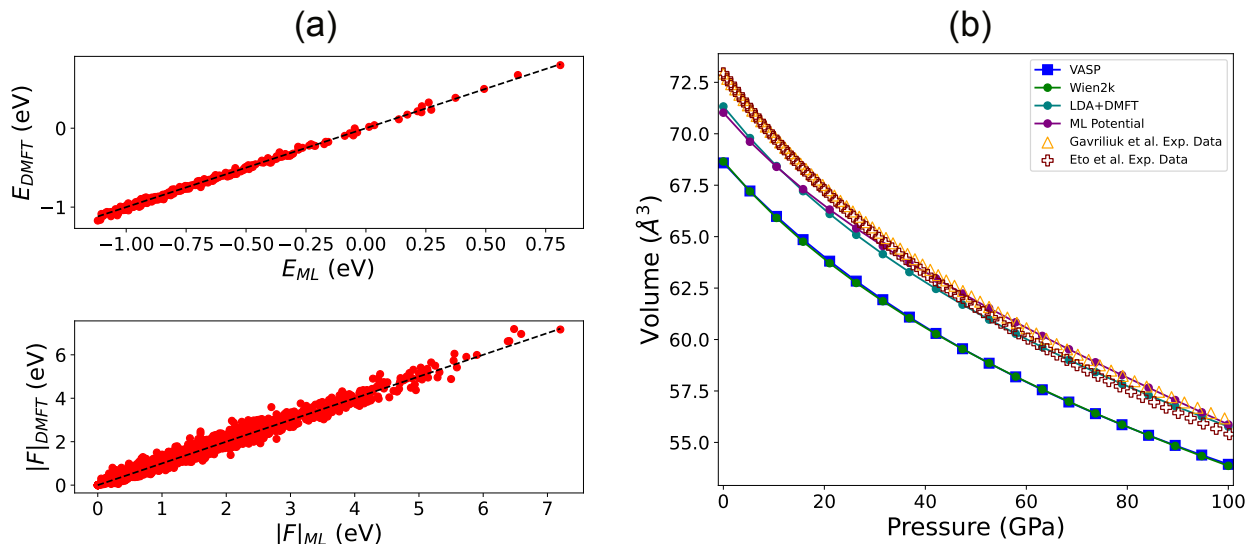


FIG. 3. (a) Internal energies and forces predicted by the MLIP versus energies and forces from LDA+DMFT. Black dashed line represents perfect agreement. (b) Comparison of equilibrium volumes of FCC phase of NiO under pressure from various first-principles programs to machine learning prediction and to experimental volume relations generated from the Birch–Murnaghan equation of state as reference. Yellow triangles were obtained by fitting parameters from Ref. [55] while the purple crosses were obtained by fitting parameters from Ref. [66].

Ce at higher temperatures. This observation aligns with the established phase diagram and supports the hypothesis that the α'' phase is a metastable state at higher temperatures [72]. The scarcity of the α'' phase at such temperatures can be attributed to the role of thermal energy in favoring the orthorhombic phase, even with a marginally higher reaction barrier. We also track entropy across the transition pathway as shown in Fig. 2c at a temperature of 400 K. Entropy calculations further elucidate the phase stability, revealing higher entropy for the α' phase, which corroborates its thermal stabilization. The intermediate phases between α and α' also have higher entropies than those in the $\alpha \rightarrow \alpha''$ pathway, indicating that the reaction barrier will likely continue decreasing as temperature increases. We report only the 400 K run results for the entropy calculations as CTQMC cannot accurately measure electronic entropy contributions at low temperature [45].

Building upon our insights from elemental Ce, we extend our investigation to NiO, a prototypical Mott insulator emblematic of strongly correlated compounds. First studied in the 1930s [78–80], the unique properties of NiO are the result of the strong correlation among its $3d$ electrons [81, 82]. Experimentally, it has been established that NiO remains insulating under extremely high pressures [83], and NiO can be considered as a representative compound for the behavior of correlated materials under the extreme conditions found within the Earth. Accurate predictions of large-scale thermal properties, such as melting curves, are essential for understanding the structure inside the Earth. These properties, however, are challenging to calculate with conventional DFT due

to its failure to accurately describe the ground state of strongly correlated materials [84, 85].

Addressing these challenges, we use graph neural networks trained on energies and forces from LDA+DMFT calculations. DMFT inherently includes the dynamical correlation effects in the many-body Hamiltonian, offering an accurate and mostly pressure independent prediction of electronic properties. This approach benefits from the inclusion of many-body effects in force calculations, potentially leading to significant structural insights when contrasted with standard DFT predictions [86]. To ensure sufficient transferability, the MLIP is trained on a variety of data generated by random structure searching as well as energy versus volume data generated from the face centered cubic ($Fm\bar{3}m$), trigonal ($R\bar{3}m$), and body centered cubic ($Pm\bar{3}m$) structures. The accuracy of the machine learning network is depicted in Fig. 3a, showing close alignment between the predicted and actual energies and forces.

Figure 3b shows the equilibrium volume predictions under varying pressures for the face-centered cubic phase of NiO, as derived from various computational methods and techniques. Wien2k and VASP were both run with the PBESol GGA exchange correlation functional. The MLIP shows good agreement with LDA+DMFT calculations in a wide pressure range, indicating a high degree of accuracy. Notably, both the MLIP and LDA+DMFT calculations surpass the traditional DFT predictions from Wien2k and VASP when compared to the experimental data. The MLIP provides an energy versus volume curve in good agreement with that from LDA+DMFT, yet it achieves this at a significantly reduced computa-

tional cost.

Next, we performed molecular dynamics calculations to estimate the melting curve of NiO under high pressures. Theoretical studies on the melting curves of strongly correlated materials are rare, due to the challenges associated with accurately simulating these phenomena across different pressure conditions. Leveraging a neural network that directly predicts energies and forces enables us to perform supercell calculations more cost-effectively than traditional DFT, while still capturing some of the force renormalization effects.

For our melting curve investigation, we used the Z method owing to its efficiency and proven reliability in experimental comparisons [87–90]. Focusing on high-temperature conditions, we constructed $3 \times 3 \times 3$ supercells derived from the face-centered cubic structure for our molecular dynamics simulations in the NVE ensemble with a spread of initial temperatures from a Maxwell-Boltzmann distribution. Since NiO transitions from a face-centered cubic ($Fm\bar{3}m$) phase above its Neel temperature of 525 K to an antiferromagnetically distorted trigonal ($R\bar{3}m$) phase only below the Neel temperature [66, 91], the starting structure should not alter the results of the molecular dynamics simulation. The system was allowed to equilibrate over 10 picoseconds with a timestep of 1 femtosecond, with thermal averages of relevant observables taken over the final 2 picoseconds. The curve was modeled using the Simon-Glatzel equation, a method that has been successful with other transition metal compounds [92–95], represented as:

$$T_m = 2172.42 \left(1 + \frac{P}{95.85}\right)^{0.5993}$$

Fig. 4 presents the melting curve of NiO in Pressure-Temperature (PT) space, mapped using isochores of 70 \AA^3 , 65 \AA^3 , and 60 \AA^3 . The MLIP effectively captures the melting behavior of NiO, with the predicted melting curve aligning well with experimental data at atmospheric pressure [96]. The alignment of the MLIP with experimental data suggests a reliable model for predicting the behavior of strongly correlated materials under extreme conditions akin to those deep within the Earth. Therefore, this approach, integrating data from DMFT into graph neural networks, offers a novel and efficient pathway to explore the complex melting behavior of strongly correlated materials like NiO.

In summary, we have demonstrated the utility of MLIPs in accelerating investigations of dynamics of correlated systems. For Cerium, training data for the MLIP was generated using the LDA+Gutzwiller method, as generation of force data from DMFT for f -electron compounds with significant spin-orbit coupling is beyond our computational capabilities. The finite difference method was used to calculate forces and stresses, and these in

turn were used to predict viable transition pathways between intermediate pressure phases of Cerium. The resulting transition pathway supports the claim that the α'' phase is more stable than α' -Ce at low temperatures. The

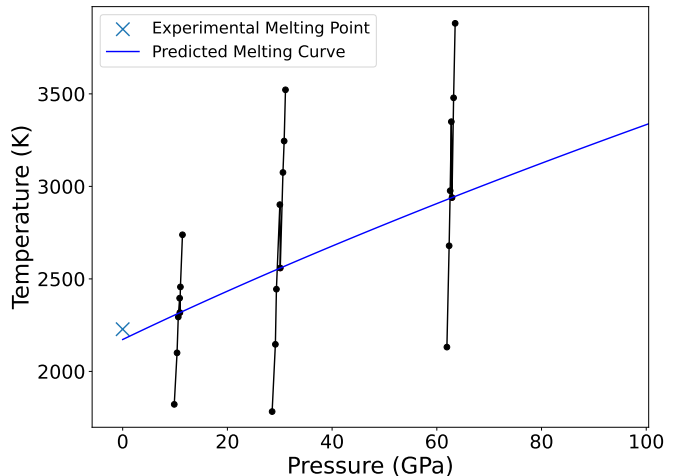


FIG. 4. Melting curve in Pressure-Temperature space. Shown in black are the Z-method curves for 3 isochores at 70 \AA^3 , 65 \AA^3 , and 60 \AA^3 in order of increasing pressure.

transition barrier to the α' phase decreases with increasing temperature while the Gibbs free energy of the α' phase decreases significantly below that of the α'' phase at high temperatures. Given the larger reaction barrier to the α' phase at both low and high temperatures however, it is no surprise that experiments commonly measure a large coexistence region. For NiO, full DMFT calculations became feasible due to the smaller orbital size and reduced effect of spin-orbit coupling. While still quite expensive to converge, training data of both energies and forces are obtained and an ML interatomic potential is trained on this data. Molecular dynamics simulations are carried out to determine the melting point of this material, with good agreement to the experimental ambient-pressure melting temperature. We hope in the future that more MLIPs can be trained for correlated systems, unlocking new avenues of transition state searching, theoretical thermodynamic predictions, and eventually crystal structure prediction of strongly correlated systems.

This work was supported by the startup funds of the office of the Dean of SASN of Rutgers University-Newark. The authors acknowledge the Office of Advanced Research Computing (OARC) at Rutgers for providing access to the Amarel cluster and associated research computing resources.

[1] N. F. Mott and Z. Zinamon, *Rep. Prog. Phys.* **33**, 881 (1970).

[2] D. Belitz and T. R. Kirkpatrick, *Rev. Mod. Phys.* **66**,

- 261 (1994).
- [3] G. R. Stewart, *Rev. Mod. Phys.* **56**, 755 (1984).
- [4] Q. Si and F. Steglich, *Science* **329**, 1161 (2010).
- [5] R. Rao and L. Zhu, *Phys. Rev. B* **108**, 235101 (2023).
- [6] J. Zakrzewski and D. Delande, *Phys. Rev. B* **98**, 014203 (2018).
- [7] J. S. Evans, C.-L. Cheng, and T. Van Voorhis, *Phys. Rev. B* **78**, 165108 (2008).
- [8] D. M. Cleland, E. K. Fletcher, A. Kuperman, and M. C. Per, *J. Phys. Mater.* **3**, 025006 (2020).
- [9] S. Ray, P. Mahadevan, A. Kumar, D. D. Sarma, R. Cimino, M. Pedio, L. Ferrari, and A. Pesci, *Phys. Rev. B* **67**, 085109 (2003).
- [10] N. Molinari, J. P. Mailoa, N. Craig, J. Christensen, and B. Kozinsky, *J. Power Sources* **428**, 27 (2019).
- [11] J. Timoshenko, A. Anspoks, A. Kalinko, and A. Kuzmin, *Acta Mater.* **129**, 61 (2017).
- [12] K. Yamaguchi, Y. Takahara, T. Fueno, and K. Nasu, *Jpn. J. Appl. Phys.* **26**, L2037 (1987).
- [13] A. Paul and T. Birol, *Annu. Rev. Mater. Res.* **49**, 31 (2019).
- [14] A. Georges, G. Kotliar, W. Krauth, and M. J. Rozenberg, *Rev. Mod. Phys.* **68**, 13 (1996).
- [15] U. Schollwöck, *Rev. Mod. Phys.* **77**, 259 (2005).
- [16] A. Baiardi and M. Reiher, *J. Chem. Phys.* **152**, 040903 (2020).
- [17] X. Deng, L. Wang, X. Dai, and Z. Fang, *Phys. Rev. B* **79**, 075114 (2009).
- [18] K. M. Ho, J. Schmalian, and C. Z. Wang, *Phys. Rev. B* **77**, 073101 (2008).
- [19] B. Himmetoglu, A. Floris, S. de Gironcoli, and M. Cococcioni, *Int. J. Quantum Chem.* **114**, 14 (2014).
- [20] R. C. Albers, N. E. Christensen, and A. Svane, *J. Phys. Condens. Matter* **21**, 343201 (2009).
- [21] R. Adler, C.-J. Kang, C.-H. Yee, and G. Kotliar, *Rep. Prog. Phys.* **82**, 012504 (2018).
- [22] E. Pavarini, *Riv. Nuovo Cimento* **44**, 597 (2021).
- [23] P. Werner, A. Comanac, L. de' Medici, M. Troyer, and A. J. Millis, *Phys. Rev. Lett.* **97**, 076405 (2006).
- [24] V. Turkowski, DMFT Impurity Solvers, in *Dynamical Mean-Field Theory for Strongly Correlated Materials* (Springer International Publishing, Cham, 2021) pp. 147–200.
- [25] E. Gull, P. Werner, S. Fuchs, B. Surer, T. Pruschke, and M. Troyer, *Comput. Phys. Commun.* **182**, 1078 (2011).
- [26] T. Yanai, Y. Kurashige, W. Mizukami, J. Chalupský, T. N. Lan, and M. Saitow, *Int. J. Quantum Chem.* **115**, 283 (2015).
- [27] S. K. Panda, H. Jiang, and S. Biermann, *Phys. Rev. B* **96**, 045137 (2017).
- [28] B. Amadon, *J. Phys. Condens. Matter* **24**, 075604 (2012).
- [29] A. Hariki, A. Hausoel, G. Sangiovanni, and J. Kuneš, *Phys. Rev. B* **96**, 155135 (2017).
- [30] W. Metzner and D. Vollhardt, *Phys. Rev. Lett.* **62**, 324 (1989).
- [31] J. Bünemann and F. Gebhard, *Phys. Rev. B* **76**, 193104 (2007).
- [32] N. Lanatà, Y. Yao, X. Deng, V. Dobrosavljević, and G. Kotliar, *Phys. Rev. Lett.* **118**, 126401 (2017).
- [33] G. Wang, Y. Qian, G. Xu, X. Dai, and Z. Fang, *Phys. Rev. Lett.* **104**, 047002 (2010).
- [34] M.-F. Tian, H.-F. Song, H.-F. Liu, C. Wang, Z. Fang, and X. Dai, *Phys. Rev. B* **91**, 125148 (2015).
- [35] M.-F. Tian, X. Deng, Z. Fang, and X. Dai, *Phys. Rev. B* **84**, 205124 (2011).
- [36] F. Lu, J. Zhao, H. Weng, Z. Fang, and X. Dai, *Phys. Rev. Lett.* **110**, 096401 (2013).
- [37] T. Schickling, F. Gebhard, J. Bünemann, L. Boeri, O. K. Andersen, and W. Weber, *Phys. Rev. Lett.* **108**, 036406 (2012).
- [38] S. Zhou and Z. Wang, *Phys. Rev. Lett.* **105**, 096401 (2010).
- [39] N. Lanatà, H. U. R. Strand, G. Giovannetti, B. Hellsing, L. de' Medici, and M. Capone, *Phys. Rev. B* **87**, 045122 (2013).
- [40] C. Herzberg, P. D. Asimow, D. A. Ionov, C. Vidito, M. G. Jackson, and D. Geist, *Nature* **493**, 393 (2013).
- [41] W. McDonough and S. s. Sun, *Chem. Geol.* **120**, 223 (1995), chemical Evolution of the Mantle.
- [42] M. J. Walter, *J. Petrol.* **39**, 29 (1998).
- [43] P. Blaha, K. Schwarz, F. Tran, R. Laskowski, G. K. H. Madsen, and L. D. Marks, *J. Chem. Phys.* **152**, 074101 (2020).
- [44] K. Haule, C.-H. Yee, and K. Kim, *Phys. Rev. B* **81**, 195107 (2010).
- [45] K. Haule and T. Birol, *Phys. Rev. Lett.* **115**, 256402 (2015).
- [46] K. Haule, *Phys. Rev. B* **75**, 155113 (2007).
- [47] K. Haule and G. L. Pascut, *Phys. Rev. B* **94**, 195146 (2016).
- [48] N. Lanatà, Y. Yao, C.-Z. Wang, K.-M. Ho, and G. Kotliar, *Phys. Rev. X* **5**, 011008 (2015).
- [49] N. Lanatà, Y.-X. Yao, C.-Z. Wang, K.-M. Ho, J. Schmalian, K. Haule, and G. Kotliar, *Phys. Rev. Lett.* **111**, 196801 (2013).
- [50] N. Lanatà, Y.-X. Yao, C.-Z. Wang, K.-M. Ho, and G. Kotliar, *Phys. Rev. B* **90**, 161104 (2014).
- [51] C. Chen and S. P. Ong, *Nat. Comput. Sci.* **2**, 718 (2022).
- [52] G. Henkelman, B. P. Uberuaga, and H. Jónsson, *J. Chem. Phys.* **113**, 9901 (2000).
- [53] L. V. Pourovskii, B. Amadon, S. Biermann, and A. Georges, *Phys. Rev. B* **76**, 235101 (2007).
- [54] K. Haule, T. Birol, and G. Kotliar, *Phys. Rev. B* **90**, 075136 (2014).
- [55] A. G. Gavriluk, V. V. Struzhkin, A. G. Ivanova, V. B. Prakapenka, A. A. Mironovich, S. N. Aksenov, I. A. Troyan, and W. Morgenroth, *Commun. Phys.* **6**, 23 (2023).
- [56] A. H. Larsen, J. J. Mortensen, J. Blomqvist, I. E. Castelli, R. Christensen, M. Dułak, J. Friis, M. N. Groves, B. Hammer, C. Hargus, *et al.*, *J. Phys. Condens. Matter* **29**, 273002 (2017).
- [57] A. B. Belonoshko, N. V. Skorodumova, A. Rosengren, and B. Johansson, *Phys. Rev. B* **73**, 012201 (2006).
- [58] A. B. Belonoshko, L. Burakovsky, S. P. Chen, B. Johansson, A. S. Mikhaylushkin, D. L. Preston, S. I. Simak, and D. C. Swift, *Phys. Rev. Lett.* **100**, 135701 (2008).
- [59] G. Kresse and J. Hafner, *Phys. Rev. B* **47**, 558 (1993).
- [60] G. Kresse and J. Furthmüller, *Comput. Mater. Sci.* **6**, 15 (1996).
- [61] G. Kresse and J. Furthmüller, *Phys. Rev. B* **54**, 11169 (1996).
- [62] P. E. Blöchl, *Phys. Rev. B* **50**, 17953 (1994).
- [63] G. Kresse and J. Hafner, *J. Phys. Condens. Matter* **6**, 8245 (1994).
- [64] G. Kresse and D. Joubert, *Phys. Rev. B* **59**, 1758 (1999).
- [65] J. P. Perdew, A. Ruzsinszky, G. I. Csonka, O. A. Vydrov, G. E. Scuseria, L. A. Constantin, X. Zhou, and K. Burke,

- Phys. Rev. Lett.* **100**, 136406 (2008).
- [66] T. Eto, S. Endo, M. Imai, Y. Katayama, and T. Kikegawa, *Phys. Rev. B* **61**, 14984 (2000).
- [67] D. C. Koskenmaki and K. A. Gschneidner, Cerium, in *Handbook on the Physics and Chemistry of Rare Earths*, Vol. 1 (Elsevier, 1978) Chap. 4, pp. 337–377.
- [68] M. Krisch, D. L. Farber, R. Xu, D. Antonangeli, C. M. Aracne, A. Beraud, T.-C. Chiang, J. Zarestky, D. Y. Kim, E. I. Isaev, R. Ahuja, and B. Johansson, *Proc. Natl. Acad. Sci.* **108**, 9342 (2011).
- [69] J. Kim, D.-C. Ryu, C.-J. Kang, K. Kim, H. Choi, T.-S. Nam, and B. I. Min, *Phys. Rev. B* **100**, 195138 (2019).
- [70] S. Eryigit, C. Parlak, and R. Eryigit, *J. Phys. Condens. Matter* **34**, 295402 (2022).
- [71] L. Huang and H. Lu, *Phys. Rev. B* **99**, 045122 (2019).
- [72] K. A. Munro, D. Daisenberger, S. G. MacLeod, S. McGuire, I. Loa, C. Popescu, P. Botella, D. Errandonea, and M. I. McMahon, *J. Phys. Condens. Matter* **32**, 335401 (2020).
- [73] B. Johansson, W. Luo, S. Li, and R. Ahuja, *Sci. Rep.* **4**, 6398 (2014).
- [74] M. I. McMahon and R. J. Nelmes, *Phys. Rev. Lett.* **78**, 3884 (1997).
- [75] J. Olsen, L. Gerward, U. Benedict, and J.-P. Itié, *Physica B+C* **133**, 129 (1985).
- [76] Y. Zhao and W. Holzapfel, *J. Alloys Compd.* **246**, 216 (1997).
- [77] G. Gu, Y. K. Vohra, and K. E. Brister, *Phys. Rev. B* **52**, 9107 (1995).
- [78] J. H. de Boer and E. J. W. Verwey, *Proc. Phys. Soc.* **49**, 59 (1937).
- [79] N. F. Mott and R. Peierls, *Proc. Phys. Soc.* **49**, 72 (1937).
- [80] N. F. Mott, *Proc. Phys. Soc. Sect. A* **62**, 416 (1949).
- [81] A. G. Gavriliuk, I. A. Trojan, and V. V. Struzhkin, *Phys. Rev. Lett.* **109**, 086402 (2012).
- [82] V. I. Anisimov, M. A. Korotin, and E. Z. Kurmaev, *J. Phys. Condens. Matter* **2**, 3973 (1990).
- [83] A. G. Gavriliuk, V. V. Struzhkin, A. G. Ivanova, V. B. Prakapenka, A. A. Mironovich, S. N. Aksenov, I. A. Troyan, and W. Morgenroth, *Commun. Phys.* **6**, 23 (2023).
- [84] M. J. DelloStritto, A. D. Kaplan, J. P. Perdew, and M. L. Klein, *APL Mater.* **11**, 060702 (2023).
- [85] J. Gebhardt and C. Elsässer, *J. Phys. Condens. Matter* **35**, 205901 (2023).
- [86] E. Plekhanov, P. Hasnip, V. Sacksteder, M. Probert, S. J. Clark, K. Refson, and C. Weber, *Phys. Rev. B* **98**, 075129 (2018).
- [87] A. B. Belonoshko and A. Rosengren, *Phys. Rev. B* **85**, 174104 (2012).
- [88] J. A. Moriarty, R. Q. Hood, and L. H. Yang, *Phys. Rev. Lett.* **108**, 036401 (2012).
- [89] J. Bouchet, F. Bottin, G. Jomard, and G. Zérah, *Phys. Rev. B* **80**, 094102 (2009).
- [90] A. Karavaev, V. Dremov, and T. Pravishkina, *Comput. Mater. Sci.* **124**, 335 (2016).
- [91] A. Mandziak, G. D. Soria, J. E. Prieto, P. Prieto, C. Granados-Mirallas, A. Quesada, M. Foerster, L. Aballe, and J. de la Figuera, *Sci. Rep.* **9**, 13584 (2019).
- [92] D. Errandonea, *Phys. Rev. B* **87**, 054108 (2013).
- [93] R. Hrubciak, Y. Meng, and G. Shen, *Nat. Commun.* **8**, 14562 (2017).
- [94] P. Parisiades, F. Cova, and G. Garbarino, *Phys. Rev. B* **100**, 054102 (2019).
- [95] A. Dewaele, M. Mezouar, N. Guignot, and P. Loubeyre, *Phys. Rev. B* **76**, 144106 (2007).
- [96] W. M. Haynes, ed., Physical constants of inorganic compounds, in *CRC Handbook of Chemistry and Physics* (CRC Press, Boca Raton, 2016) pp. 4–75, 97th ed.